Chemical Engineering Journal 486 (2024) 149915

Contents lists available at ScienceDirect

Chemical Engineering Journal

journal homepage: www.elsevier.com/locate/cej

Implementing water recirculation in a novel portable plasma-activated water reactor enhances antimicrobial effect against *Escherichia coli*☆

Rita Agus [a,*], Fabio Avino [a,1], Lorenzo Ibba [a,1], Brayden Myers [a], Leonardo Zampieri [b], Emilio Martines [b], Alan Howling [b], Ivo Furno [a]

[a] Ecole Polytechnique Fédérale de Lausanne (EPFL), Swiss Plasma Center (SPC), Lausanne, CH-1015, Switzerland
[b] University of Milano - Bicocca, Department of Physics "G. Occhialini", Piazza della Scienza 3, Milano, 20126, Italy

ARTICLE INFO

Keywords:
Plasma-activated water
Surface dielectric barrier discharge
Water recirculation impact on PAW chemistry
Reactive oxygen and nitrogen species
Decontamination
Reactor design and characterization

ABSTRACT

The need for sustainable and reliable decontamination methods is driven by concerns regarding antibiotic resistance, as well as environmental and cost-efficiency challenges associated with traditional methods. Plasma-activated water (PAW) holds significant promise as an innovative and eco-friendly decontamination method. Nevertheless, prior to industrial implementation of PAW-based decontamination devices, a deep understanding of the bacterial inactivation mechanisms and its interplay with PAW chemical composition is required. Advancing in this field requires interdisciplinary and collaborative research using standardized practices with cost-effective and shareable PAW reactors that are still missing today. Here, to this end, a portable PAW reactor, featuring a surface dielectric barrier discharge (SDBD) that operates in air, is presented. The gaseous and aqueous phases were chemically characterized by Fourier transform infrared (FTIR) absorption spectroscopy and vis-spectrophotometry, respectively. To assess PAW antimicrobial efficacy *Escherichia coli* was employed as a model organism on six different PAW samples for three different treatment times. The significance of water recirculation in controlling the chemical composition of PAW, altering the nitrogen species balance in favor of NO_2^-, is demonstrated. This chemical modification consequently enhanced the antimicrobial effectiveness of PAW, reaching a log reduction of ~6. Exposing *E. coli* to equivalent concentrations of RONS to those found in PAW attained similar log-reductions, indicating that acidified nitrites are key to PAW antimicrobial activity. Through an innovative and portable design, this study illustrates the crucial role of water recirculation in tailoring PAW composition, leading to improved decontamination capabilities and establishing a key parameter for further optimization of PAW production.

1. Introduction

In recent years, plasma-activated water (PAW), generated through the interaction of cold atmospheric plasmas (CAPs) with water, has been investigated for various applications in the agricultural [1–4] and biomedical fields [5–7]. Plasma, the fourth state of matter, is an ionized gas abundant in positive and negative ions, electrons, and reactive radicals. It is characterized by the presence of electromagnetic radiation and strong electric fields [5]. CAPs are classified as non-thermal plasmas, meaning that electrons and heavy particles, such as ions and neutral species, do not reach thermal equilibrium. While the electron temperature is of the order of $\sim 10^4$ K, enabling high temperature chemical reactions, the temperature of heavy particles, which defines the gas temperature, remains close to room temperature. This ensures that CAPs are well-suited for heat-sensitive and biological applications [8,9]. When CAPs interact with liquids, the reactive oxygen and nitrogen species (RONS) produced by the plasma in air enter the liquid phase [6]. PAW has gained recognition in the plasma medicine field for its antimicrobial properties as an environmentally-friendly and cost-effective decontamination agent [10–12]. These qualities are due to the transient chemical activity of PAW, the employment of air and water as the primary precursors instead of potentially hazardous or expensive chemicals, and the relatively low cost of a PAW reactor [5,13]. The antimicrobial properties of PAW have been extensively linked to the synergistic effect of RONS [14,15], which can be classified into two groups: short-lived and long-lived species. The former primarily consists of OH, NO, O_2^-, $OONO_2^-$ and $ONOO^-$, and are characterized by half-lifetimes between 1 ns and a few seconds [5]. They are considered

☆ Electronic Supplementary Information (ESI) available: ESI.

* Corresponding author.
E-mail address: rita.agus@epfl.ch (R. Agus).

[1] These authors contributed equally to this work.

https://doi.org/10.1016/j.cej.2024.149915
Received 14 November 2023; Received in revised form 8 February 2024; Accepted 20 February 2024
Available online 23 February 2024

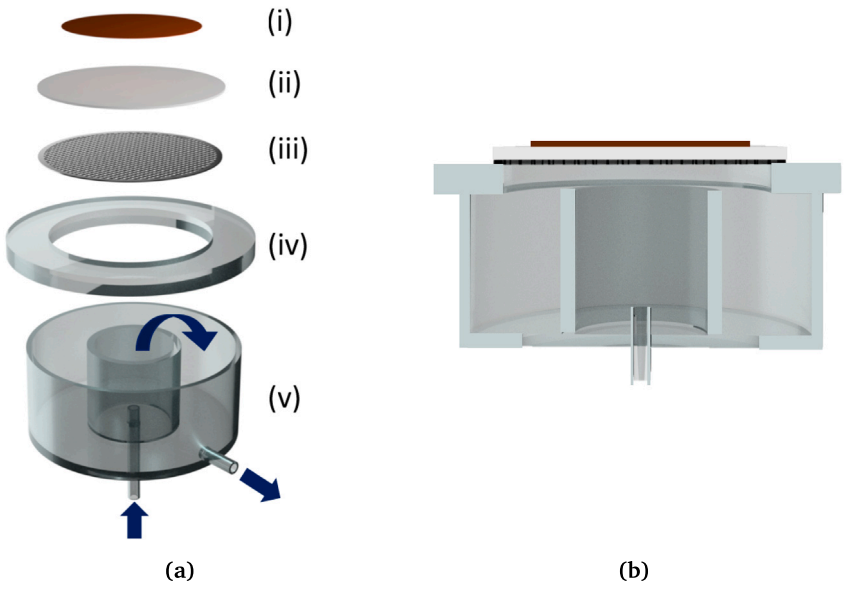

Fig. 1. Expanded (a) and assembled not to scale (b) view of the plasma-activated water reactor setup. The SDBD features a copper back-plate electrode (i), a 1 mm thick alumina disk (ii) and a stainless steel perforated disk electrode (iii). The SDBD is located on top of an 8 mm thick glass spacer (iv) and held together by a 3D-printed support (omitted for simplification). The glass spacer is in contact with a glass vessel (v). Blue arrows indicate the water flow direction.

crucial when treating biological samples immersed in liquids directly in contact with CAPs. The latter, mainly O_3, NO_3^-, NO_2^- and H_2O_2, have half-lifetimes that span from minutes to years, and are of greater significance in post-discharge applications of PAW [6].

As research into its potential applications has continued, PAW has become an excellent candidate to address the public health requirements associated with novel antibacterial agents [13,16]. It is well documented that antibiotic resistance poses a significant challenge to global health, food security, and overall development, driving research towards new decontamination methods [17]. Preliminary studies have observed that bacteria exposed to CAPs or plasma-treated liquids do not show persistence in subsequent treatments [18], nor do they develop resistance when survivors are used to produce the next generation of bacteria to be treated [19]. It has also been demonstrated that CAPS are effective against both antibiotic-resistant and non-resistant bacteria, likely because of the bacterial degradation induced during plasma treatment [20]. In this context, understanding PAW inactivation mechanisms, identifying the chemical species responsible and exploring methods to enhance their production are essential steps. These insights will allow for the optimization of PAW production depending on the specific application and the characteristics of the target microorganisms.

One of the remarkable features of PAW is the sensitivity to the specific configuration of the plasma reactor employed for its production [21]. This sensitivity extends to the ensuing water chemistry, which in turn influences its antimicrobial efficacy [22]. Numerous studies have investigated how the reactor configuration impacts the chemical composition and biological effects of PAW. Firstly, the PAW chemistry is influenced by the discharge location with respect to the liquid. This includes: indirect modes where plasmas are produced above the water [23], multiphase discharges (*e.g.* plasma ignited within bubbles [24]), and plasmas ignited directly within a liquid solution [5,6,21]. Nevertheless, several additional factors significantly influence the composition of PAW. Rothwell et al. [25] proved that extending the duration of water exposure and increasing the frequency of the discharge enhances the bactericidal impact of PAW. The antimicrobial activity of PAW is also affected by the working gas, such as N_2 or O_2 [26] or different $O_2/(O_2 + N_2)$ ratios [27]. The application of nobles gases, like helium [26] and argon [25], or Ar + N_2 + O_2 mixtures [28] has also been explored. Zhou et al. [26] demonstrated that using air as operating gas, as opposed to O_2, N_2 and He, produced more long-lived RONS, ultimately leading to a better decontamination of mung bean. For practical and economic considerations, air is the most widely adopted working gas [29]. The electrodes design and the ground layout, whether on surface dielectric barrier discharge SDBD [23], spark discharge [30], pin-to-liquid discharge [24], just to give a few examples, can also drastically influence the plasma chemistry and in turn the composition of PAW [15,31]. Furthermore, in a study conducted by Machala et al. [30], the air flow rate was found to affect the PAW composition. They demonstrated that lower flow rates guaranteed more NO and NO_2 formation due to the accumulation of the reactive species in the reactor. Kim et al. [32] showed, instead, the possibility to selectively produce NO, NO_2 or O_3 by increasing the flow rate in an air-flowing SDBD reactor.

Additionally, the initial chemical properties of water have an impact on the composition of PAW. For example, Rothwell et al. [25] demonstrated that the pH decreased rapidly when Milli-Q water was used, while it would not be altered in tap water. Likewise, the input power deeply influences the properties of the plasma discharge, defining a more oxigen- or nitrogen-oxides oriented chemistry for higher power densities [33].

Multiple studies have shown that the condition and duration of PAW storage can affect the antimicrobial effect. An et al. [34] demonstrated that in case of deionized water treatment the antimicrobial effect on *E. coli* O157:H7 was not modified when storing PAW an open or closed reactor, but it would affect the efficacy of NaOCl treated solutions. Shen et al. [35] investigated the impact of storage temperature on the antibacterial activity of PAW. They found that samples stored at −80 °C maintained higher antibacterial activity compared to samples stored at −20 °C, 4 °C and 25 °C for a duration of 30 days. Consistent with these findings, additional studies have shown that lower temperatures are more efficient in preserving both the effectiveness of inactivation and the concentration of reactive nitrogen species in PAW [36]. Furthermore, it has been observed that the antimicrobial effect of PAW diminishes as storage time increases [37].

Various plasma-based designs may be found in the literature that utilize water recirculation to enhance the mixing of the liquid sample. The study conducted by Punith et al. [38] investigated the feasibility of utilizing a recirculating pump–spray system in an arc plasma discharge reactor, equipped with an underwater electrode, to increase the growth

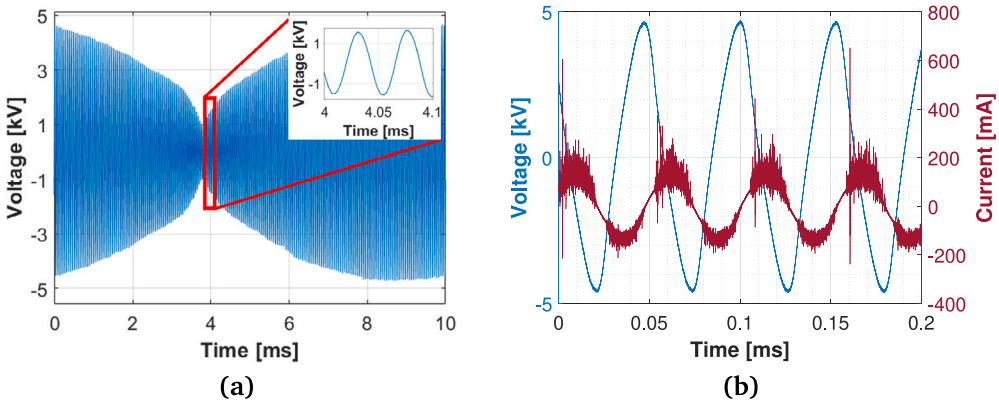

Fig. 2. Voltage waveform with a zoom for the visualization of the excitation frequency (a). Voltage and current diagram (b).

of tomato plants. Experimental analysis and mathematical simulation of a water falling dielectric barrier discharge (DBD) reactor, used for the degradation of pollutants in liquids, shown that by recirculating the water for 10 cycles, it was possible to accumulate NO_3^- ions. However, the concentrations of H_2O_2 and O_3, reached saturation after the initial cycle of operation in an air environment [39,40].

Despite the large variety of PAW studies, to the best of our knowledge, the correlation between PAW chemistry and antimicrobial efficacy in samples generated with and without water recirculation using a SDBD has not been investigated thus far.

This study showcases a novel and portable setup that is ideal for on-site treatments and shareable among different laboratories. We provide evidence of the significant impact of water recirculation on the chemical composition of PAW and its profound influence on the accumulation of NO_2^- and NO_3^-. The PAW, produced by the exposure of ultra-pure water to an over-water SDBD operated at ~39 W, delivered promising results on *E. coli* inactivation. The two investigated configurations, with and without the water flow, are referred to as dynamic and static modes. During indirect water treatment, mainly long-lived RONS can diffuse and dissolve into the liquid phase and are considered relevant for post-discharge PAW applications [6]. As such, samples were chemically characterized in terms of O_3, NO_2^-, NO_3^- and H_2O_2 through vis-spectrophotometry [21,41]. PAW physical properties, such as oxidation–reduction potential (ORP), pH and electrical conductivity (EC) were also measured. The influence of the plasma exposure duration on the chemical composition was evaluated by characterizing water samples exposed to the plasma for 10, 20, and 30 minutes. To gain a deeper understanding of the gaseous chemistry that leads to the generation of aqueous RONS, *in-situ* Fourier transform infrared (FTIR) absorption spectroscopy was performed, allowing the quantification of O_3, NO_2 and N_2O. The results of gaseous phase and PAW characterization are presented in Sections 3.1 and 3.2 respectively. The antimicrobial properties of static and dynamic PAW against *E. coli* were assessed for different bacteria treatment durations (10, 30 and 50 minutes), to explore how variations in chemical composition translate to distinct antimicrobial outcomes.

Understanding PAW interaction with bacteria is crucial for advancing this technology. In this context, the question regarding the possibility of achieving comparable antimicrobial results when mimicking PAW composition remains a topic of ongoing debate. Prior research has demonstrated discrepancies between artificial and actual PAW [7,41–43]. On the other hand, similar outcomes could be achieved by mimicking the composition of PAW in other works [23]. To clarify whether this was possible for our reactor configuration, the chemical composition of the most aggressive PAW sample, generated by 30-minute exposure to plasma in dynamic configuration, was mimicked and tested on *E. coli* in Section 3.4, obtaining similar inactivation.

In this work, we proved that the presence of water recirculation has a notable impact on the concentration of reactive nitrogen species (RNS) measured in PAW, leading to a significant increase in RNS levels during dynamic operations. This translates to enhanced antimicrobial efficacy, providing a foundation for the development of more efficient and portable PAW reactors utilizing SDBD technologies for antimicrobial applications.

2. Experimental

2.1. Plasma-activated water reactor setup

Fig. 1 shows the PAW reactor configuration used for the indirect treatment of water with a SDBD. The SDBD consisted of a 0.2 mm thick copper tape layer as back-plate (diameter 59 mm), an alumina disk 1 mm thick (diameter 80 mm, purity 99.6%) and a 0.5 mm thick stainless steel perforated disk electrode with an 80 mm diameter and a mesh size of 2 mm. Using a 3D-printed support, the SDBD was mounted on top of an 8 mm thick glass spacer. The spacer was in contact with the glass vessel, creating a closed environment between the SBDB and the vessel, without any external air flow (Fig. 1(b)). The glass spacer also maintains a gap between the plasma discharge and the water, ensuring that the transport of RONS to the liquid phase occurs exclusively through diffusion from the gas phase. The glass vessel was designed with two concentric pools with internal diameters of 37 mm and 100 mm. A video showing the reactor assembly is available in the supplementary material.†

During plasma treatment the water was contained in the glass vessel and recirculated through the two pools as shown by the blue arrows in Fig. 1(a). The water circuit inlet was located at the bottom of the reactor forcing the water to flow upwards, through the internal pool and towards the SDBD, then downwards to the external pool. The inlet and outlet were connected by PTFE tubing to a peristaltic pump, with a constant flow rate of 200 mL/min. The choice of materials in contact with the water – glass and PTFE – was made based on their chemical inertness, ensuring that they would not interfere with the composition of the PAW. The volume of water treated in this work was 150 mL, however, larger volumes could be treated given that the glass vessel has a capacity of 0.3 L. This reactor configuration offers modularity and scalability, allowing for the connection of multiple reactors in series. A number of parameters can be modified with this setup: the distance between the water and the SDBD depending on the spacer thickness, the volume of water treated, the pumping speed, the power supply and the SDBD configuration. This design is also highly portable, with all essential components, including the reactor vessel, SDBD, pump, tubing, and power supply, compactly fitting into a 10 L container.

The power supply employed was a commercially available ozone generator, adapted for this application. The circuit schematic is reported in the supplementary material†. The high voltage waveform (Fig. 2(a)) featured an 8.8 kV peak-to-peak wave at 21 kHz, modulated

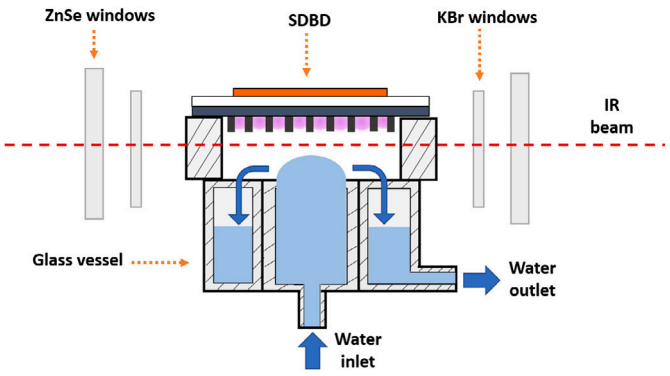

Fig. 3. Schematic of the frontal section of the *in-situ* FTIR the setup (not to scale).

at 100 Hz. Fig. 2(b) shows the voltage and current diagram over 0.2 ms of discharge.

The discharge power, measured by Lissajous figures, was ~39 W with an associated surface power density of 1.43 W/cm^2 [44–46]. The power was monitored every 30 s for 10, 20 and 30 minutes of continuous discharge, indicating fluctuations within 4%. The discharge power did not change when the reactor was operated with or without water and in static or dynamic conditions. Moreover, the discharge was not susceptible to humidity, presumably thanks to the applied voltage and to the back-plate heating attained by plasma operation [46], reaching ~120 °C within a few minutes of operation.

2.2. Gaseous phase characterization

An *in-situ* FTIR absorption spectroscopy configuration, shown in Fig. 3, was used to examine the primary reactive species produced by the SDBD plasma operated in air [47,48]. The *in-situ* method provides the advantage of direct measurements of the plasma species that come into contact with the water. The PAW reactor was placed within a stainless steel chamber located in the sample compartment of a Bruker Vertex 80v FTIR absorption spectrometer, sealed by two 49.5 mm diameter ZnSe windows. [49] To protect these windows, and to confine the gaseous plasma products within the inner chamber, supplementary KBr windows of 22.5 mm diameter were installed on opposing ports of the chamber itself [47,48]. The glass spacer supporting the SDBD was modified with two holes for the FTIR measurements to allow for the passage of the infrared beam. The infrared beam is Gaussian, with a diameter of around 8 mm. During the measurements the beam axis is positioned approximately 4 mm below the DBD. The other ports of the stainless steel reactor were used for the electrical connections and the water circuit. Due to these connections, the sample compartment was kept open during the spectra acquisition causing the IR beam to propagate over a brief distance through the ambient air between the external windows, leading to spurious CO_2 signal around 2300 cm^{-1}.

Each IR spectrum consisted of 10 averaged scans, and the absorbance was computed with respect to a background acquired before switching on the plasma. A spectrum was acquired every 15 s for 10 minutes of plasma operation. The spectral data were analyzed and compared to standard spectra for each gas. The absolute calibration of the infrared signal was accomplished using the Beer–Lambert law [50]. The concentration in parts per million (ppm) for a particular molecule was calculated by the following formula:

$$n_i = \frac{A(\nu)}{\sigma_i(\nu)L}\left(\frac{10^6}{n}\right) \quad (1)$$

where $A(\nu) = \ln(I_0/I)$ is the absorbance as a function of wavenumber ν, I_0 is the radiant power of incident light on the sample, I is the radiant power transmitted by the sample, L is the length pathway of the infrared beam in the reactor and $\sigma_i(\nu)$ is the absorption cross section of the chemical species i. The last term $10^6/n$ serves as conversion factor from molecules/cm^3 to ppm, with n representing the gas density. The absorption cross-section values for particular molecules, such as O_3, NO_2 and N_2O were obtained from the HITRAN database [51]. No discernible traces of HNO_3, H_2O_2, NO, and N_2O_5, typically detected in FTIR of CAPs [21,30,48,52], were observed in the spectra. These signals were most likely masked by the noise originating from the presence of water in the vessel.

2.3. Evaluation of PAW physical and chemical properties

PAW physical properties were measured with three dedicated probes connected to a metrohm-914 analogic pH/conductometer with an integrated temperature sensor: a Platinum ring electrode for redox potential measurements, a Unitrode pH electrode and a conductivity measuring cell electrode [53].

PAW long-lived species concentrations (H_2O_2, NO_3^-, NO_2^- and O_3) were measured by vis-spectrophotometry (Spectroquant® Prove 100, Merck). H_2O_2 measurements were performed with the Spectroquant® Hydrogen Proxide Test (1.18789.0001) using the 10 mm quartz cell with an associated accuracy of ±0.07 mg/l. This method is based on the reduction of copper(II) ions to copper(I) ions by hydrogen peroxide in the presence of phenanthroline derivative, forming an orange-colored complex that was measured photometrically [54]. The selectivity of the phenanthroline method to quantify H_2O_2 in the presence of NO_2^- was confirmed through a comparative analysis. H_2O_2 concentrations were measured in deionized water samples prepared using only H_2O_2, as well as samples containing both H_2O_2 and NO_2^-, resulting in interference-free measurements.

NO_3^- concentrations were measured with Spectroquant® Nitrate Cell Test (1.14563.0001) with an associated accuracy of ±0.5 mg/l. In sulfuric and phosphoric solutions, nitrate ions react with 2,6-dimethylphenol (DMP) to form 4-nitro-2,6-dimethylphenol, a pink compound whose concentration was determined photometrically [55].

Measurements of nitrite ions were performed with the Spectroquant® Nitrite Cell Test (1.00609.0001) with an associated accuracy of ±2.8 mg/l. In acidic solution nitrite ions react with iron(II) ethylenediammonium sulfate to form a yellow to green-brown iron(II) compound [56]. MQuant® Peroxide-Test (1.10081.0001), MQuant® Nitrit-Test (1.10007.0001), and MQuant® Nitrat-Test (1.10020.0001) test strips were used to confirm the respective order of magnitude of the H_2O_2, NO_3^- and NO_2^- measurements.

The Spectroquant® Ozone Test (1.00607.0002) was employed for O_3 measurements using the 10 mm and 50 mm quartz cells. This method is based on the reaction of ozone with dipropyl-p-phenylenediamine (DPD) in weakly acidic solution to form a red-violet dye that was determined photometrically [57]. The reliability of this method is discussed in Section 3.2.

The chemical characterization was performed on PAW samples immediately after plasma exposure. Ultra-pure water produced by a Puranity TU 3UV/UF+ water dispenser was used as initial sample, with a pH~ 6, ORP ~320 mV and EC ~0.055 µScm^{-1}.

PAW samples are named by the acronym PAW-X, where X indicates that the ultra-pure water is plasma-treated for X minutes.

2.4. Preparation of solutions mimicking PAW composition

Nitrite standard solution 1000 mg/l (1.19899), nitrate standard solution 1000 mg/l (1.19811), sulfuric acid (1.09072) and hydrogen peroxide solution 30% (1.07210), purchased by Merck, were utilized to prepare solutions with chemical properties matching those of dynamic PAW-30 [58]. These solutions were employed to quantify the impact of the individual chemical species on *E. coli* inactivation. [41]

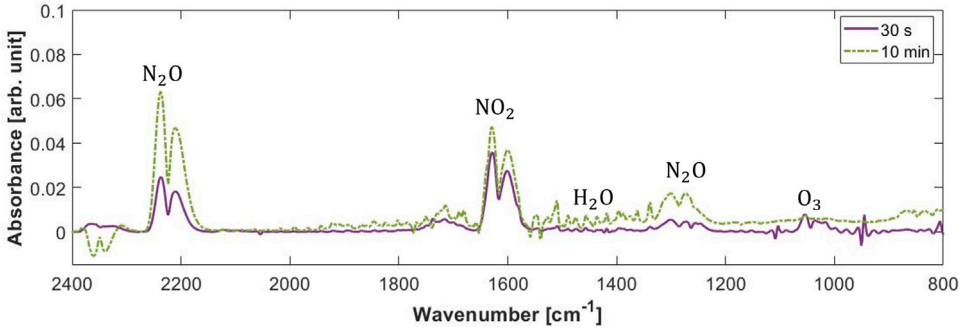

Fig. 4. Representative FTIR spectra, acquired after 30 s (solid line) and 10 minutes (dashed line) of plasma operation in the dynamic configuration.

2.5. Microbiological protocol

The effect of PAW was tested on *Escherichia coli* K-12 strain MG1655. Bacteria cell stocks stored in a solution of Luria–Bertani (LB) medium and glycerol (% 30 v/v) at −80 °C were used for the preparation of an overnight culture by inoculating 100 µl of cell stocks into 10 ml of LB and then incubating at 37 °C and 180 rpm for at least 8 h. The bacteria culture was reactivated by inoculating 10 µl of overnight culture into 10 ml of fresh LB and again incubating at 37 °C and 180 rpm. The optical density (OD) at 600 nm of the reactivated solution was measured to determine the growth phase of the cells. Experiments were performed with bacteria cultures having an OD_{600} between 0.2 and 0.5, associated with a concentration of approximately 10^7 CFU/ml [59,60]. For PAW treatment, 1 ml of bacteria suspension was centrifuged at 4000 rpm for 3 min, 960 µL of supernatants were removed and the pellet was re-suspended in 960 µL of PAW. Bacteria were incubated at 37 °C and 180 rpm during PAW treatment. Although it may enhance the depletion of reactive nitrogen species and hence hinder the impact of PAW, this temperature has been selected as it is ideal for *E. coli* replication [35,36]. At the end of the treatment time, cells were centrifuged and the PAW was removed. The pellet was re-suspended in LB, serially diluted in 10-folds and plated on agar for colony forming unit (CFU) counting. Plates were incubated at 37 °C for 8 h. CFUs were counted and checked again 24 h after the experiment. The same process was performed on control cells by re-suspension in deionized water instead of PAW. The antibacterial effect was quantified by the log reduction, $log(N_0/N)$, where N_0 is the population of the control sample, and N is the number of viable cells after exposure to PAW [61,62]. The tubes used for bacteria centrifuging and PAW exposure were 1.5 mL micro tubes purchased from Thermo Fisher Scientific (3641NK). [63]

2.6. Statistical analysis

The statistical analysis was performed using the statistical program CoStat software version 6.45. Different treatments were compared using analysis of variance (ANOVA). Significant differences were identified by the Student–Newman–Keuls multiple range test, with a confidence level of $p \leq 0.05$. [35,64]

3. Results and discussion

3.1. FTIR results

In Fig. 4, two representative FTIR spectra are shown, acquired after 30 s and 10 minutes of plasma discharge in the dynamic configuration, suggesting a RNS buildup and O_3 minimization during operation. The data were corrected for the baseline drift of the spectra, visible in the second half of the figure. This drift is mainly caused by mechanical vibrations of the experimental setup, involving both the spectrometer and the PAW reactor [47,48,65]. The detailed N_2O, NO_2 and O_3 concentration kinetics during 10 minutes of plasma discharge are shown

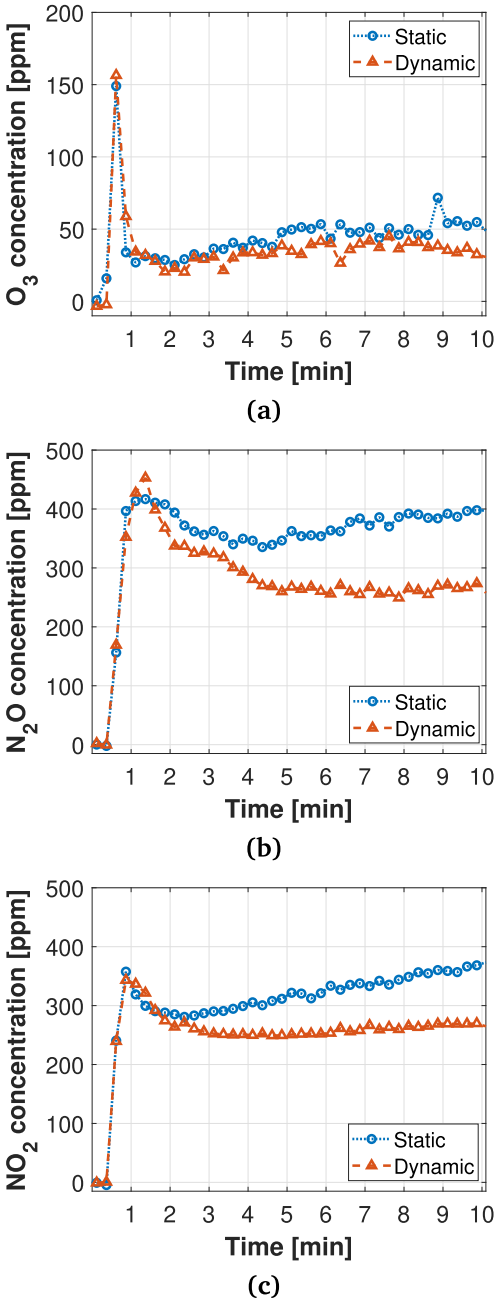

Fig. 5. Time evolution of O_3 (a), N_2O (b) and NO_2 (c) concentrations measured by *in-situ* FTIR in static and dynamic configuration.

in Fig. 5. O_3 levels, shown in Fig. 5(a), did not exhibit any differences between static and dynamic operation. Initially, O_3 concentrations increased up to 150 ppm, followed by a decline to ~40 ppm within 40 to 50 s into the discharge period, which is likely attributable to O_3 quenching by nitrogen species [33,66]. As illustrated in Fig. 5(b), the N_2O concentration exhibited a similar initial trend in both static and dynamic operations, reaching 400 ppm within the first minute of the discharge. During static operation, the N_2O concentration stabilized at 400 ppm, while in dynamic operation it decreased to around 300 ppm. Concentrations of NO_2, showed in Fig. 5(c), also increased during the first minute of plasma operation, then dropped slightly, before rising again to higher values (~390 ppm) in static operation.

The gaseous phase characterization by FTIR confirmed a nitrogen oxides-dominated chemistry, as expected, given the relatively high surface power density of the plasma discharge (1.43 W/cm^2).[33] During static operation the higher concentrations of N_2O and NO_2 observed can be ascribed to the longer residence times of these species in the gaseous phase. In contrast, the water recirculation enhanced these species transfer into the liquid, inducing lower gaseous concentrations. The water recirculation did not have a significant impact on O_3 kinetics. This is likely because O_3 is quickly quenched by nitrogen species within the first minute of the discharge, and hence its chemistry is not influenced by the water conditions. Previous studies proved that in nitrogen oxides-modes O_3 immediately reacts with NO, oxidizing it into NO_2.[32] In high humidity environments, O_3 depletion can also be associated to reactions with OH radicals.[67]

The effect of these differences on PAW chemical composition is discussed in Section 3.2.

3.2. PAW physicochemical characterization

Results of PAW physicochemical characterization for static and dynamic PAW samples, for different treatment times, are reported in Fig. 6. Water recirculation did not significantly affect pH, ORP or EC, but rather the concentration of long-lived RNS.

The pH of all samples (Fig. 6(a)) decreased from the initial value of ~ 6, reaching 3.5 after 10 minutes and a minimum of 3 after 30 minutes of plasma treatment. Concurrently, the EC (Fig. 6(b)) increased with plasma exposure, rising from ~0.055 μScm^{-1} to 150 μScm^{-1} after 10 minutes, and further to an average of 400 μScm^{-1} following 30 minutes of treatment. ORP denotes the tendency of a solution towards oxidation or reduction, with higher ORP values signifying a more oxidizing nature [68]. As already mentioned, ultra-pure water typically exhibits an ORP of approximately 320 mV, and during plasma treatment it increased in both static and dynamic samples, reaching 530 mV for PAW-10 and peaking at 565 mV for PAW-30 (Fig. 6(c)).

Fig. 6(d) shows that during static operations the H_2O_2 concentration increased from 0.11 mgL^{-1} after 10 minutes of treatment to 0.25 mgL^{-1} following 30 minutes of plasma exposure. In the case of dynamic samples, the H_2O_2 concentration was 1.5 to 2 times the static one, reaching a maximum of 0.45 mgL^{-1} after 20 minutes of plasma exposure.

In Fig. 6(e) and (f), the NO_2^- and NO_3^- concentrations are shown. The RNS increased with plasma exposure time, proving that these species can be accumulated in PAW [7], but in different proportions depending on the water flow. In dynamic samples, the balance of nitrogen species was altered in favor of NO_2^-, resulting in nitrite concentrations from 2 to 2.5 times the static configuration for all treatment durations. The highest concentration of NO_2^- was approximately 55 mgL^{-1} in dynamic PAW-30, followed by 40 mgL^{-1} and 17 mgL^{-1} in the case of 20 and 10 minutes of plasma exposure. For static PAW, NO_2^- concentrations were 21 mgL^{-1}, 17 mgL^{-1}, and 11 mgL^{-1} after 30, 20, or 10 minutes of plasma treatment, respectively.

In all static samples, NO_3^- was the dominant species, reaching an average of 1.5 times the NO_2^- concentration. The NO_3^- concentration increased from 15 mgL^{-1} after 10 minutes of treatment to nearly 60 mgL^{-1} after 30 minutes of exposure to plasma. With water recirculation, NO_3^- exhibited variations from 12 to 42 mgL^{-1} with longer treatment time from 10 to 30 minutes. Fig. 7 shows the evolution of the ratio NO_2^-/NO_3^- in static and dynamic configurations for all plasma exposure durations. Independent of the duration of the plasma treatment, NO_2^- was found to be 1.4 times NO_3^- in the case of dynamic PAW. Conversely, in static samples, this ratio was much lower, decreasing from 0.71 after 10 minutes of plasma treatment to 0.38 after 30 minutes.

In general, water recirculation augmented the total concentration of nitrogen ions (NO_2^- + NO_3^-) by 10% in PAW-10 and 25% in PAW-20 and PAW-30. This enhancement in liquid RNS during dynamic operation correlates well with the FTIR results described in Section 3.1. In agreement with the surface-renewal theory of interphase transport, the mass transfer of reactive species from the gaseous phase is enhanced in the presence of a turbulent flow of the liquid, due to increased mixing and continuous renewal of the interface [69,70]. The lower concentrations of gaseous NO_2 and N_2O, and the higher concentration of liquid RNS measured with water recirculation, is presumably a consequence of the more efficient transport to the liquid of NxOy. In the static configuration, RONS transport is mediated by molecular diffusion, associated to the establishment of a concentration gradient to drive the mass transfer process.

Among long-lived species, the determination of O_3 in air plasma-treated water can be affected by fast decay and low-selectivity in the presence of H_2O_2 and OH [21,30,71]. The indigo blue assay is the most utilized quantitative colorimetric standardized method for ozone detection in water and wastewater [72], but it can provide unreliable results for plasma-treated samples [71]. In this work, we tested the DPD method for ozone detection in PAW, already in use in the water analysis and plasma-treated water fields [72–75]. Ozone concentrations in the samples were expected to be negligible, since FTIR measurements confirmed a RNS-oriented chemistry. Furthermore, the Henry's law constant for O_3 is much smaller than that of most other gaseous RONS produced by a DBD plasma [76]. The residual ozone in the liquid phase would promptly oxidize nitrites, which are among the predominant species in this reactor configuration, with a pH-dependent reaction [30,71,77]:

$$NO_2^- + O_3 \longrightarrow NO_3^- + O_2 \qquad k_c = 5.8 \cdot 10^5\ \mathrm{M\,sec}^1 \tag{2}$$

The NO_2^- measured by spectrophotometry refers to the total amount of nitrite ions present in PAW, $[NO_2^-]_{tot}$. Depending on the pH, part of these ions do not affect the ozone consumption since they are involved in the equilibrium reaction with HNO_2 (Eq. (3)) with an acid dissociation constant (pk_a) of 3.29.

$$HNO_2 \rightleftharpoons NO_2^- + H^+ \qquad pK_a = 3.29 \tag{3}$$

$$\frac{[NO_2^-][H^+]}{[HNO_2]} = 10^{-pK_a} \tag{4}$$

By rearranging Eq. (4) and (6) it is possible to estimate the amount of NO_2^- involved in the equilibrium reaction:

$$[NO_2^-] = \frac{10^{-pK_a}[NO_2^-]_{tot}}{[H^+] + 10^{-pK_a}} \tag{5}$$

Therefore, to calculate the consumption of ozone, the concentration of nitrite to consider is:

$$[NO_2^-] = [NO_2^-]_{tot} - [HNO_2] \tag{6}$$

Following these equations, the O_3 half-life in solution containing NO_2^- can be estimated by [72]:

$$\frac{-d[O_3]}{dt} = k_c[O_3] \cdot [NO_2^-] \tag{7}$$

$$[O_3] = [O_3]_0 e^{-k_c[NO_2^-]t} \tag{8}$$

$$t_{1/2}(O_3) = -\frac{log(\frac{1}{2})}{k_c[NO_2^-]} \tag{9}$$

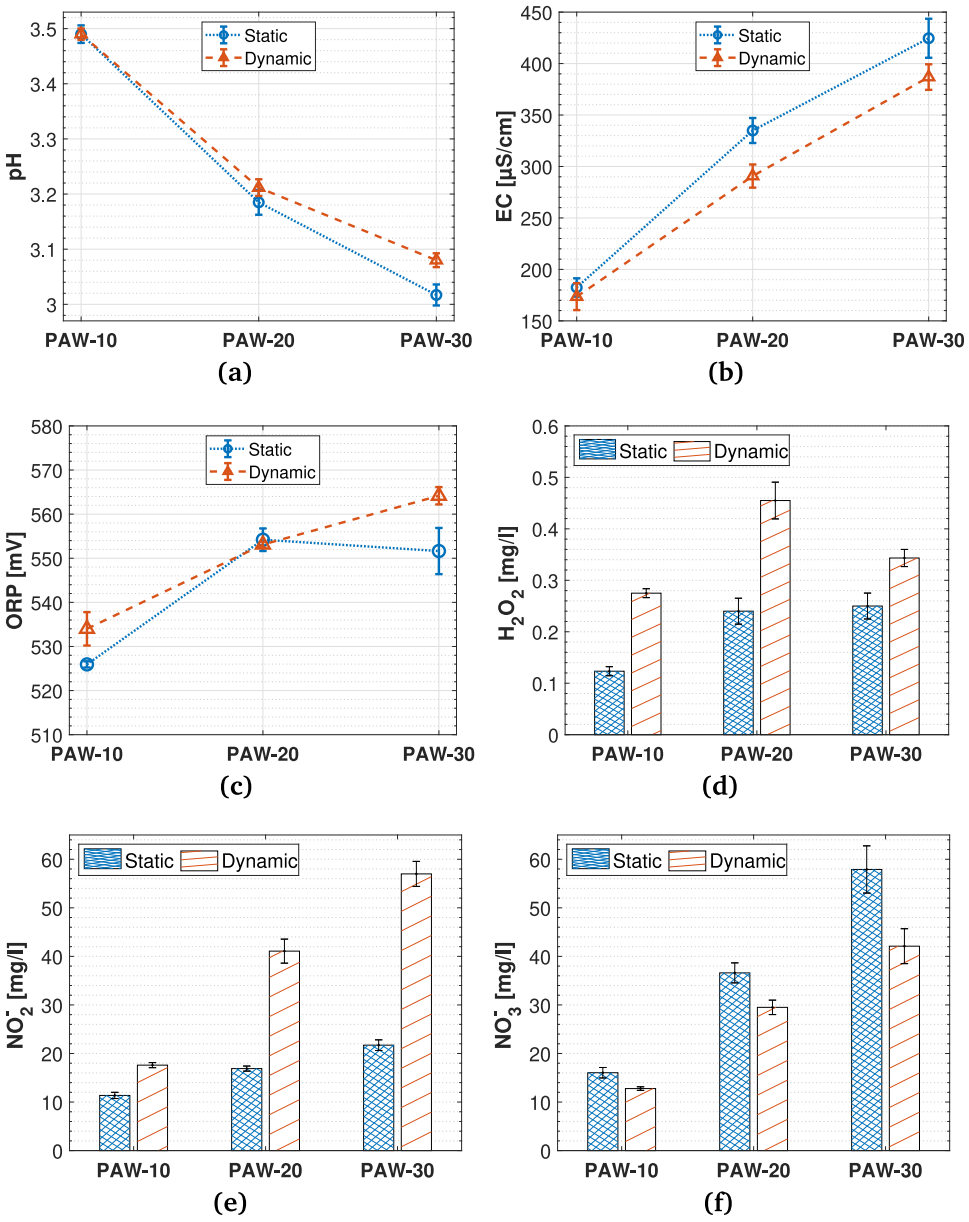

Fig. 6. pH (a), electrical conductivity (EC) (b), oxidation–reduction potential (ORP) (c), H_2O_2 (d), NO_2^- (e), and NO_3^- (f) concentrations measured in the static and dynamic configurations for 10, 20 and 30 minutes of plasma exposure. Plots represent the average of the replicates and the error bars represent ± the standard error of the mean.

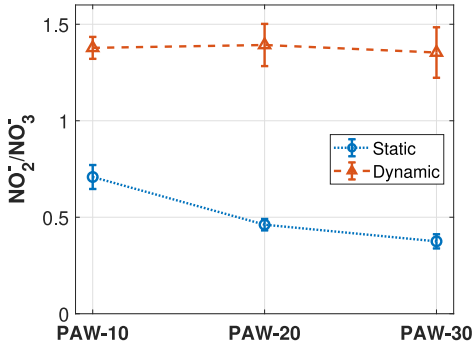

Fig. 7. The ratio of nitrite and nitrate as a function of plasma treatment time in the static and dynamic water treatment configurations. Plots represent the average and the error bars represent ± the standard error of the mean.

To assess the reliability of the DPD method, the ozone half-life determined by Eq. (9) has been compared with DPD measurements for dynamic PAW-30. In this case, the ozone half-life obtained is 2.6 ms, in disagreement with the ozone measurements performed with the DPD method where O_3 concentrations only decreased 13% (from 2.3 mgL^{-1} to 2 mgL^{-1}), in the 30 minutes following plasma treatment.

The DPD method was also tested on solutions containing nitrate, nitrite and hydrogen peroxide in the same amount as dynamic PAW-30. The ozone concentration measured by DPD was identical to the reading obtained for the actual PAW sample, despite no O_3 being added to the water solutions mimicking dynamic PAW-30. These results confirmed that the ozone concentrations in the PAW samples produced by this reactor configuration are null and the obtained results were artifacts, likely due to the poor selectivity of the method with respect to other oxidants (NO_2^-, H_2O_2 and possibly ONOOH). It is therefore worth noting possible inaccuracies of the DPD method in complex samples such as PAW. Figures showing the erroneous measurements of O_3 using DPD are reported in the supplementary material†.

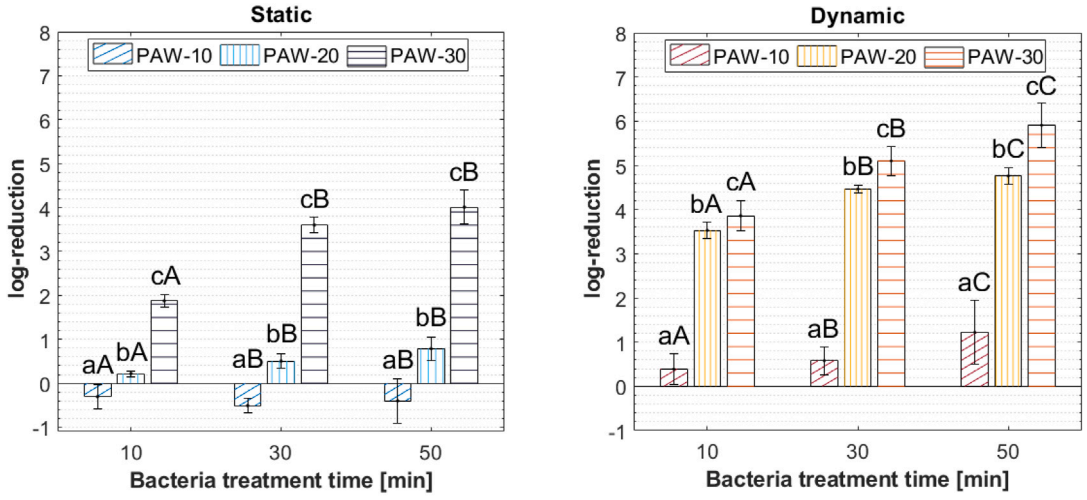

(a) (b)

Fig. 8. *E. coli* log reduction for 10, 30 and 50 minutes of bacteria treatment time by PAW-10, PAW-20 and PAW-30 with static (a) or dynamic (b) PAW. Plots represent the average of 3 replicates and the error bar represents ± the standard error of the mean. Different lowercase letters for the same bacteria treatment times indicate significant differences among different PAW samples ($p \leq 0.05$). Different capital letters indicate significant differences among different bacteria treatment time for the same PAW sample ($p \leq 0.05$).

3.3. *E. coli* treatment with static and dynamic PAW samples

Static and dynamic samples of PAW-10, PAW-20 and PAW-30 have been tested on *E. coli* to assess the antimicrobial effect for 10, 30 and 50 minutes of bacteria treatment time. 1 mL of bacteria suspension was treated with 960 µL of fresh PAW extracted from the reactor. The results are summarized in Fig. 8. Dynamic samples (Fig. 8(b)) resulted in higher log reductions with respect to the static ones (Fig. 8(a)), for all bacteria treatment times. The antimicrobial activity of static and dynamic samples increased with the duration of the water exposure to the plasma, leading to highest efficacy for PAW-30 in both operational modes. For the static PAW-10 scenario, the obtained negative log reduction mean suggests treatment ineffectiveness. Bacteria in contact with PAW multiplied, resulting in a higher colony count compared to the control group. Static PAW-20 and PAW-30 exhibited significant disparities in their antimicrobial efficacy. The former achieved less than a 0.8-log reduction for all bacteria treatment durations, whereas the latter displayed the highest efficiency within the static samples, leading to reductions ranging from 1.8-log to 4-log with increasing bacteria treatment time. It should be noted that for static PAW the differences in the results for bacteria treatment times of 30 and 50 minutes were not statistically significant ($p \leq 0.05$). On the contrary, in the case of dynamic PAW, bacterial treatment duration of 10, 30, or 50 minutes exhibited statistically different outcomes, with longer treatment times yielding higher log reductions. Dynamic PAW-30 antimicrobial efficacy ranged from 3.8-log reduction after 10 minutes of bacteria exposure, to 5.1-log and 6-log reduction for treatments lasting 30 and 50 minutes, respectively. In this same configuration, PAW-20 antimicrobial efficacy was slightly lower with 3.5-log, 4.4-log, 4.7-log for 10, 30 or 50 minutes of bacteria exposure. Dynamic PAW-10 proved to be the least aggressive dynamic sample, with 0.4-log, 0.6-log, and 1.2-log reductions for 10, 30 or 50 minutes of contact time.

As discussed in Section 3.2, static and dynamic samples differed mostly on the chemical composition but not in terms of pH, EC and ORP. This implies that the differences in microbiological effects were primarily linked to the differences in RONS abundance, rather than pH, EC and ORP. More specifically, the dynamic water treatment strongly modified the NO_2^- and NO_3^- chemistry leading to samples richer in NO_2^-. This change corresponded to different rates of bacterial inactivation for the same plasma discharge parameters and energy consumption, proving that dynamic PAW exhibits greater antimicrobial capacity with shorter bacteria treatment times.

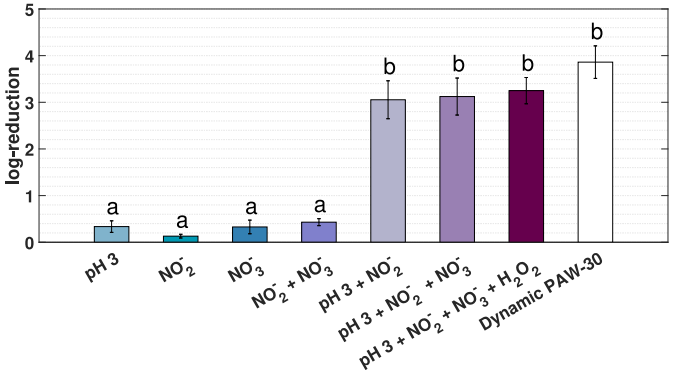

Fig. 9. The log reduction measured after 10 minutes of bacteria treatment with different combinations of RONS and pH mimicking dynamic PAW-30, compared with the log reduction observed for actual PAW-30. Values plotted represent the average of 3 replicates and the error bars represent ± the standard error of the mean. Different lowercase letters indicate significant differences ($p \leq 0.05$).

3.4. Comparison of dynamic PAW-30 and solutions mimicking its composition on bacteria inactivation

Evaluating the impact of particular chemical species is crucial for comprehending the mechanisms involved in the antimicrobial properties of PAW. Previous studies revealed different bacteria inactivation when comparing artificial and actual PAW [7,41,42]. In contrast, other works could obtain comparable effects when mimicking PAW composition [23]. Here, the efficacy of the most aggressive antimicrobial PAW sample (dynamic PAW-30) is compared to mimicking solutions over a 10-minute duration. As shown in Fig. 9, to assess the influence of the reactive species and pH, various combinations were tested. The average inactivation obtained for 10 minutes treatment with dynamic PAW-30 was 3.86-log. The reference dynamic PAW-30 parameters used for the preparation of the solutions are reported in Table 1. A log reduction of less than 0.5 was measured for *E. coli* exposed to NO_2^- and NO_3^- alone or combined, in a neutral pH. Bacteria suspended in a solution with a pH of 3 exhibited an average reduction of only 0.3-log. This finding aligns with the documented acid tolerance of *E. coli* [78,79]. As also reported by Oehmigen et al. exposing *E. coli* to a solution with a pH of 3 in the absence of plasma-generated RONS does not yield the

Table 1
Dynamic PAW-30 reference characteristics used for the preparation of PAW-mimicking solutions.

NO_2^- (mgL^{-1})	NO_3^- (mgL^{-1})	H_2O_2 (mgL^{-1})	pH
54	41	0.35	3

same inactivation effect as plasma-treated liquids [41,42]. Higher log reductions, of the order of 3.05-log, were obtained by the combination of low pH and NO_2^-. As already mentioned, since the pK_a of HNO_2 is 3.29 [80], the combination of pH 3 and NO_2^- is favorable to keep most NO_2^- in the form of molecular nitrous acid/free nitrous acid (FNA) (Eq. (3)). FNA is unstable and decomposes into nitrogen oxides by direct disproportionation:

$$3HNO_2 \longrightarrow H^+ + NO_3^- + 2NO + H_2O \quad (10)$$

or through a series of reactions that produce NO and NO_2 as intermediaries, which are thought to be responsible for FNA cytotoxicity. [14,67,80,81][82] FNA is known to provoke strong nitrosative stress on the structural components of the cell envelope, possibly causing cell lysis and increasing cell membrane permeability due to damage/perforations in the cell envelope, as well as biofilm dispersal via extracellular polymeric matrix breakdown [83–85]. In solutions where NO_3^- was also added, an average reduction of 3.12-log was measured, suggesting a minimal contribution from NO_3^- on the inactivation. The closest effect to that of PAW was observed when H_2O_2 was included in the combination of low pH, NO_2^-, and NO_3^-, resulting in a log reduction of 3.25. Under these conditions, the prerequisites for the formation of peroxynitrite were met. Peroxynitrite is known for its strong cytotoxic effect, possibly explaining the slightly higher log reduction. [7,14,67]

Fig. 9 shows that the effect of NO_2^- when combined with NO_3^- and H_2O_2 did not show statistically significant differences, indicating that nitrous acid is the key component for the antimicrobial effect on *E. coli*. In addition, the log reduction achieved with dynamic PAW-30 is statistically equivalent to the solutions replicating PAW composition in an acidic environment ($p \leq 0.05$). To summarize, this study suggests that in this configuration NO_2^- primarily contributes to the inactivation of *E. coli*, and that the low pH is a necessary but not a sufficient condition for PAW antimicrobial activity. Moreover, solutions designed to mimic the composition of PAW produced comparable results in terms of bacterial inactivation.

4. Conclusions

Plasma-activated water (PAW) has gained recognition as a potential novel and green decontamination method. However, in the context of practical applications, it is crucial to understand how to tailor PAW chemistry to meet specific antimicrobial requirements. Furthermore, the development of an effective but still portable and replicable PAW reactor is necessary to promote *in-situ* application and scientific collaboration, and to facilitate testing across diverse environments and applications.

In this context, we present the design of a portable PAW reactor that significantly enriches water with reactive oxygen and nitrogen species by non-contact exposure to an atmospheric surface dielectric barrier discharge. As a function of the plasma–water exposure time (10, 20 and 30 minutes), and operating with or without water flow, it was possible to produce and characterize 6 PAW samples in terms of H_2O_2, NO_2^-, NO_3^-, pH, electrical conductivity and oxidation–reduction potential. The DPD method, tested for O_3 measurements, was found to be unreliable for PAW characterization. In any case, considering the nitrogen-oxides operating mode of the reactor [33], and the NO_2^- concentrations measured, O_3aq is considered to be negligible. In support of this assumption, the half-life time of ozone has been estimated taking into account the NO_2^- average concentration and the pH of dynamic PAW-30, suggesting that ozone half-life time in water would be of the order of 2.6 ms [73].

This study particularly investigates how water recirculation affects PAW composition, as a method for chemically altering its chemical properties. In static operation, FTIR measurements showed higher levels of N_2O and NO_2, which can be attributed to the extended residence times of these species in the gaseous phase. Conversely, the recirculation of water facilitated the transfer of these species into the liquid phase, resulting in decreased gaseous concentrations. Notably, O_3 kinetics were not significantly affected by water recirculation, and in both configurations it was quenched during the first minute of discharge. Therefore, consistent with the surface-renewal theory, the water flow enhances the mass transfer of reactive species produced by the plasma into the liquid phase [69]. Specifically, it was demonstrated that the water flow induced an increase from 10% to 25% of the total concentration of $NO_2^- + NO_3^-$. More precisely, the dynamic samples demonstrated higher levels of NO_2^- and displayed greater *E. coli* inactivation.

The study of static and dynamic water treatment for different plasma exposure times revealed significant variations in *E. coli* inactivation due to the PAW chemical alteration. The log-reduction values varied by about seven orders of magnitude, ranging from less than 0.3 to around 6. By implementing water recirculation, we were able to demonstrate that the antibacterial effect of PAW may be significantly enhanced. This, in our opinion, might have a significant influence on the advancement of PAW reactors intended for antimicrobial applications.

In agreement with Park et al. [23], we demonstrated that solutions mimicking PAW composition can induce similar inactivation. Moreover, exposing bacteria to combinations of low pH, NO_2^-, NO_3^-, and H_2O_2– highlighted the key role of an acidic environment in effectively inactivating *E. coli* via acidified nitrites.

In contrast to other reactor configurations, [82,86] these findings indicate that the inactivation of *E. coli* might be caused by nitrosative stress rather than oxidative stress. Future research should aim to elucidate the bacteria inactivation pathways induced by nitrogen species in PAW, in order to clarify the underlying mechanisms and enhance the efficacy and specificity of this technology.

The authors would like to draw the attention to the fact that different microorganisms might respond differently to PAW treatment. Lavrikova et al. proved that *Escherichia coli*, a gram negative bacteria, was inactivated by cell membrane break down after the exposure to a transient spark discharge in a saline solution. On the contrary, gram positive *Staphylococcus aureus*, showed resilience to the plasma treatment for up to 20 min of exposure [87]. In the case of spores it has been demonstrated that *Bacillus cereus* inactivation by PAW can be influenced by several parameters. Specifically, higher temperatures (up to 55 °C) and lower concentrations of spores and organic interfering substances (*e.g.*, bovine serum albumin), along with a reduced treated volume, could enhance spore inactivation [88]. The bacteria state, whether planktonic or biofilm, can also significantly impact PAW antimicrobial effect, since the reactive species delivery in biofilm conditions is more challenging due to the nature of the biofilm itself [89]. On this topic, Zhou et al. demonstrated that underwater microplasma bubbles, behave as transport vehicles for RONS delivery, improving biofilm dispersion [90]. Future studies should broaden the study of PAW inactivation on different microorganisms and conditions, as a fundamental step to strengthen the knowledge of PAW inactivation mechanism.

CRediT authorship contribution statement

Rita Agus: Writing – review & editing, Writing – original draft, Methodology, Investigation, Formal analysis, Data curation, Conceptualization. **Fabio Avino:** Writing – review & editing, Resources, Conceptualization. **Lorenzo Ibba:** Writing – review & editing, Investigation,

Formal analysis. **Brayden Myers:** Writing – review & editing, Conceptualization. **Leonardo Zampieri:** Writing – review & editing. **Emilio Martines:** Writing – review & editing. **Alan Howling:** Writing – review & editing. **Ivo Furno:** Writing – review & editing, Supervision, Project administration, Funding acquisition, Conceptualization.

Declaration of competing interest

The authors declare that they have no known competing financial interests or personal relationships that could have appeared to influence the work reported in this paper.

Data availability

Data will be made available on request.

Acknowledgments

The authors express their deep gratitude to Professor Urs Von Gunten for his significant contributions on the understanding of ozone chemistry in PAW. Furthermore, we extend our acknowledgments to the skilled personnel in the electrical workshop of the Swiss Plasma Center, as well as to Eglantine Vialaneix and Maxence Calamand for their assistance in facilitating the initial measurements of this study. Special acknowledgments also go to Mr. Ralph Kastl for his impeccable manufacturing of the glass vessel for the PAW reactor. [91]

Appendix A. Supplementary data

Supplementary material related to this article can be found online at https://doi.org/10.1016/j.cej.2024.149915.

References

[1] I.K. Naumova, A.I. Maksimov, A.V. Khlyustova, Stimulation of the germinability of seeds and germ growth under treatment with plasma-activated water, Surf. Eng. Appl. Electrochem. 47 (3) (2011) 263–265, http://dx.doi.org/10.3103/S1068375511030136.

[2] A. Waskow, F. Avino, A. Howling, I. Furno, Entering the plasma agriculture field: An attempt to standardize protocols for plasma treatment of seeds, Plasma Process. Polym. 19 (1) (2022) 1–22, http://dx.doi.org/10.1002/ppap.202100152.

[3] M. Šimek, T. Homola, Plasma-assisted agriculture: history, presence, and prospects—a review, Eur. Phys. J. D 75 (7) (2021) 1–31, http://dx.doi.org/10.1140/epjd/s10053-021-00206-4.

[4] G.S. Ganesh, J. Ananthanarasimhan, P. Leelesh, H. Rao, A.M. Shivapuji, P.L. Girard-Lauriault, L. Rao, Plasma-activated water from DBD as a source of nitrogen for agriculture: Specific energy and stability studies, J. Appl. Phys. 129 (9) (2021) 093303, http://dx.doi.org/10.1063/5.0039253.

[5] R. Zhou, R. Zhou, P. Wang, Y. Xian, A. Mai-Prochnow, X. Lu, P.J. Cullen, K.K. Ostrikov, K. Bazaka, Plasma-activated water: Generation, origin of reactive species and biological applications, J. Phys. D: Appl. Phys. 53 (30) (2020) 303001, http://dx.doi.org/10.1088/1361-6463/ab81cf.

[6] A. Mai-Prochnow, R. Zhou, T. Zhang, K.K. Ostrikov, S. Mugunthan, S.A. Rice, P.J. Cullen, Interactions of plasma-activated water with biofilms: inactivation, dispersal effects and mechanisms of action, NPJ Biofilms Microbiomes 7 (1) (2021) 1–12, http://dx.doi.org/10.1038/s41522-020-00180-6.

[7] R. Zhou, R. Zhou, K. Prasad, Z. Fang, R. Speight, K. Bazaka, K. Ostrikov, Cold atmospheric plasma activated water as a prospective disinfectant: The crucial role of peroxynitrite, Green Chem. 20 (23) (2018) 5276–5284, http://dx.doi.org/10.1039/c8gc02800a.

[8] A. Fridman, G. Friedman, Plasma Medicine, Wiley, 2012, URL https://books.google.ch/books?id=QXpTD7rkrgcC.

[9] A. Fridman, L. Kennedy, Plasma Physics and Engineering, CRC Press, 2016, URL https://books.google.ch/books?id=eAJ-DwAAQBAJ.

[10] N. Basiri, M. Zarei, M. Kargar, F. Kafilzadeh, Int. J. Food Microbiol. 406 (September) (2023) 110419, http://dx.doi.org/10.1016/j.ijfoodmicro.2023.110419.

[11] Y. Zhao, M.L. Bhavya, A. Patange, D.W. Sun, B.K. Tiwari, Plasma-activated liquids for mitigating biofilms on food and food contact surfaces, Compr. Rev. Food Sci. Food Saf. 22 (3) (2023) 1654–1685, http://dx.doi.org/10.1111/1541-4337.13126.

[12] Q. Zhang, R. Ma, Y. Tian, B. Su, K. Wang, S. Yu, J. Zhang, J. Fang, Sterilization efficiency of a novel electrochemical disinfectant against *Staphylococcus aureus*, Environ. Sci. Technol. 50 (6) (2016) 3184–3192, http://dx.doi.org/10.1021/acs.est.5b05108.

[13] K. Hadinoto, B.A. Niemira, F.J. Trujillo, A review on plasma-activated water and its application in the meat industry, (22) (2023) 4993–5019, http://dx.doi.org/10.1111/1541-4337.13250.

[14] P. Lukes, E. Dolezalova, I. Sisrova, M. Clupek, Aqueous-phase chemistry and bactericidal effects from an air discharge plasma in contact with water: Evidence for the formation of peroxynitrite through a pseudo-second-order post-discharge reaction of H_2O_2 and HNO_2, Plasma Sources. Sci. Technol. 23 (1) (2014) 015019, http://dx.doi.org/10.1088/0963-0252/23/1/015019.

[15] C. Bradu, K. Kutasi, M. Magureanu, N. Puac, S. Živkovic, Reactive nitrogen species in plasma-activated water : generation, chemistry and application in agriculture, J. Phys. D: Appl. Phys. 53 (2020) 223001, http://dx.doi.org/10.1088/1361-6463/ab795a.

[16] M. Rahman, M.S. Hasan, R. Islam, R. Rana, A.S. Sayem, M.A.A. Sad, A. Matin, A. Raposo, R.P. Zandonadi, H. Han, A. Ariza-Montes, A. Vega-Muñoz, A.R. Sunny, Plasma-activated water for food safety and quality: A review of recent developments, Int. J. Environ. Res. Public Health 19 (11) (2022) 6630, http://dx.doi.org/10.3390/ijerph19116630.

[17] Antibiotic resistance, 2023, URL https://www.who.int/news-room/fact-sheets/detail/antibiotic-resistance. Accessed:2023-10-23.

[18] M.K. Nicol, T.R. Brubaker, B.J. Honish, A.N. Simmons, A. Kazemi, M.A. Geissel, C.T. Whalen, C.A. Siedlecki, S.G. Bilén, S.D. Knecht, G.S. Kirimanjeswara, Antibacterial effects of low-temperature plasma generated by atmospheric-pressure plasma jet are mediated by reactive oxygen species, Sci. Rep. 10 (1) (2020) 1–11, http://dx.doi.org/10.1038/s41598-020-59652-6.

[19] J.L. Zimmermann, T. Shimizu, H.U. Schmidt, Y.F. Li, G.E. Morfill, G. Isbary, Test for bacterial resistance build-up against plasma treatment, New J. Phys. 14 (2012) 1–16, http://dx.doi.org/10.1088/1367-2630/14/7/073037.

[20] A. Sakudo, T. Misawa, Antibiotic-resistant and non-resistant bacteria display similar susceptibility to dielectric barrier discharge plasma, Int. J. Mol. Sci. 21 (17) (2020) 1–12, http://dx.doi.org/10.3390/ijms21176326.

[21] P.J. Bruggeman, M.J. Kushner, B.R. Locke, J.G. Gardeniers, W.G. Graham, D.B. Graves, R.C. Hofman-Caris, D. Maric, J.P. Reid, E. Ceriani, D. Fernandez Rivas, J.E. Foster, S.C. Garrick, Y. Gorbanev, S. Hamaguchi, F. Iza, H. Jablonowski, E. Klimova, J. Kolb, F. Krcma, P. Lukes, Z. MacHala, I. Marinov, D. Mariotti, S. Mededovic Thagard, D. Minakata, E.C. Neyts, J. Pawlat, Z.L. Petrovic, R. Pflieger, S. Reuter, D.C. Schram, S. Schröter, M. Shiraiwa, B. Tarabová, P.A. Tsai, J.R. Verlet, T. Von Woedtke, K.R. Wilson, K. Yasui, G. Zvereva, Plasma-liquid interactions: A review and roadmap, Plasma Sources. Sci. Technol. 25 (5) (2016) 053002, http://dx.doi.org/10.1088/0963-0252/25/5/053002.

[22] P. Lukes, J.-L. Brisset, B.R. Locke, Plasma Chemistry and Catalysis in Gases and Liquids, John Wiley & Sons, Ltd, 2012, http://dx.doi.org/10.1002/9783527649525.ch8.

[23] J.Y. Park, S. Park, W. Choe, H.I. Yong, C. Jo, K. Kim, Plasma-functionalized solution: A potent antimicrobial agent for biomedical applications from antibacterial therapeutics to biomaterial surface engineering, ACS Appl. Mater. Interfaces 9 (50) (2017) 43470–43477, http://dx.doi.org/10.1021/acsami.7b14276.

[24] K. Hadinoto, J.B. Astorga, H. Masood, R. Zhou, D. Alam, P.J. Cullen, S. Prescott, F.J. Trujillo, Efficacy optimization of plasma-activated water for food sanitization through two reactor design configurations, Innov. Food Sci. Emerg. Technol. 74 (2021) 102867, http://dx.doi.org/10.1016/j.ifset.2021.102867.

[25] J.G. Rothwell, D. Alam, D.A. Carter, B. Soltani, R. McConchie, R. Zhou, P.J. Cullen, A. Mai-Prochnow, The antimicrobial efficacy of plasma-activated water against *Listeria* and *E. coli* is modulated by reactor design and water composition, J. Appl. Microbiol. (2021) http://dx.doi.org/10.1111/jam.15429.

[26] R. Zhou, J. Li, R. Zhou, X. Zhang, S. Yang, Atmospheric-pressure plasma treated water for seed germination and seedling growth of mung bean and its sterilization effect on mung bean sprouts, Innov. Food Sci. Emerg. Technol. 53 (2019) 36–44, http://dx.doi.org/10.1016/j.ifset.2018.08.006.

[27] F. Girard, M. Peret, N. Dumont, V. Badets, S. Blanc, K. Gazeli, C. Noël, T. Belmonte, L. Marlin, J.P. Cambus, G. Simon, N. Sojic, B. Held, S. Arbault, F. Clément, Correlations between gaseous and liquid phase chemistries induced by cold atmospheric plasmas in a physiological buffer, Phys. Chem. Chem. Phys. 20 (14) (2018) 9198–9210, http://dx.doi.org/10.1039/c8cp00264a.

[28] H.A.Q. Than, T.H. Pham, D.K.V. Nguyen, T.H. Pham, A. Khacef, Non-thermal plasma activated water for increasing germination and plant growth of *Lactuca sativa L*, Plasma Chem. Plasma Process. 42 (1) (2022) 73–89, http://dx.doi.org/10.1007/s11090-021-10210-6.

[29] M. Oliveira, P. Fernández-Gómez, A. Álvarez-Ordóñez, M. Prieto, M. López, Plasma-activated water: A cutting-edge technology driving innovation in the food industry, Food Res. Int. 156 (May) (2022) http://dx.doi.org/10.1016/j.foodres.2022.111368.

[30] Z. Machala, B. Tarabová, D. Sersenová, M. Janda, K. Hensel, Chemical and antibacterial effects of plasma activated water: Correlation with gaseous and aqueous reactive oxygen and nitrogen species, plasma sources and air flow conditions, J. Phys. D: Appl. Phys. 52 (3) (2019) 034002, http://dx.doi.org/10.1088/1361-6463/aae807.

[31] P. Lu, D. Boehm, P. Bourke, P.J. Cullen, Achieving reactive species specificity within plasma-activated water through selective generation using air spark and glow discharges, Plasma Process. Polym. 14 (8) (2017) 1–9, http://dx.doi.org/10.1002/ppap.201600207.

[32] J. Kim, H. Lee, S.C. Huh, J.H. Bae, W. Choe, D. Han, S. Park, S. Ryu, S. Park, Competitive formation of NO, NO_2, and O_3 in an air-flowing plasma reactor: A central role of the flow rate, Chem. Eng. J. 468 (2) (2023) 143636, http://dx.doi.org/10.1016/j.cej.2023.143636.

[33] M.J. Pavlovich, D.S. Clark, D.B. Graves, Quantification of air plasma chemistry for surface disinfection, Plasma Sources. Sci. Technol. 23 (6) (2014) 065036, http://dx.doi.org/10.1088/0963-0252/23/6/065036.

[34] J.Y. An, H.I. Yong, H.J. Kim, J.Y. Park, S.H. Lee, K.H. Baek, W. Choe, C. Jo, Estimation of inactivation effects against *Escherichia coli* O157:H7 biofilm by different plasma-treated solutions and post-treatment storage, Appl. Phys. Lett. 114 (7) (2019) 073703, http://dx.doi.org/10.1063/1.5082657.

[35] J. Shen, Y. Tian, Y. Li, R. Ma, Q. Zhang, J. Zhang, J. Fang, Bactericidal effects against *S. aureus* and physicochemical properties of plasma activated water stored at different temperatures, Sci. Rep. 6 (2016) 28505, http://dx.doi.org/10.1038/srep28505.

[36] Q. Wang, D. Salvi, Evaluation of plasma-activated water (PAW) as a novel disinfectant: Effectiveness on escherichia coli and listeria innocua, physicochemical properties, and storage stability, Lebensm.-Wiss. Technol. 149 (June) (2021) 111847, http://dx.doi.org/10.1016/j.lwt.2021.111847.

[37] M.J. Traylor, M.J. Pavlovich, S. Karim, P. Hait, Y. Sakiyama, D.S. Clark, D.B. Graves, Long-term antibacterial efficacy of air plasma-activated water, J. Phys. D: Appl. Phys. 44 (47) (2011) 3–7, http://dx.doi.org/10.1088/0022-3727/44/47/472001.

[38] N. Punith, R. Harsha, R. Lakshminarayana, M. Hemanth, M.S. Anand, S. Dasappa, Plasma activated water generation and its application in agriculture, Adv. Mater. Lett. 10 (10) (2019) 700–704, http://dx.doi.org/10.5185/amlett.2019.0042.

[39] V.V. Kovačević, B.P. Dojčinović, M. Jović, G.M. Roglić, B.M. Obradović, M.M. Kuraica, Measurement of reactive species generated by dielectric barrier discharge in direct contact with water in different atmospheres, J. Phys. D: Appl. Phys. 50 (15) (2017) http://dx.doi.org/10.1088/1361-6463/aa5fde.

[40] S. Mohades, A.M. Lietz, M.J. Kushner, Generation of reactive species in water film dielectric barrier discharges sustained in argon, helium, air, oxygen and nitrogen, J. Phys. D: Appl. Phys. 53 (43) (2020) http://dx.doi.org/10.1088/1361-6463/aba21a.

[41] K. Oehmigen, J. Winter, M. Hähnel, C. Wilke, R. Brandenburg, K.D. Weltmann, T. Von Woedtke, Estimation of possible mechanisms of *Escherichia coli* inactivation by plasma treated sodium chloride solution, Plasma Process. Polym. 8 (10) (2011) 904–913, http://dx.doi.org/10.1002/ppap.201000099.

[42] S. Ikawa, K. Kitano, S. Hamaguchi, Effects of pH on bacterial inactivation in aqueous solutions due to low-temperature atmospheric pressure plasma application, Plasma Process. Polym. 7 (1) (2010) 33–42, http://dx.doi.org/10.1002/ppap.200900090.

[43] T.P. Chen, J. Liang, T.L. Su, Plasma-activated water: antibacterial activity and artifacts? Environ. Sci. Pollut. Res. 25 (27) (2018) 26699–26706, http://dx.doi.org/10.1007/s11356-017-9169-0.

[44] F. Peeters, T. Butterworth, in: A. Nikiforov, Z. Chen (Eds.), Electrical Diagnostics of Dielectric Barrier Discharges, IntechOpen, Rijeka, 2018, http://dx.doi.org/10.5772/intechopen.80433.

[45] T.C. Manley, The electric characteristics of the ozonator discharge, Trans. Electrochem. Soc. 84 (1) (1943) 83, http://dx.doi.org/10.1149/1.3071556.

[46] F. Avino, A.A. Howling, M. Von Allmen, A. Waskow, L. Ibba, J. Han, I. Furno, Surface DBD degradation in humid air, and a hybrid surface-volume DBD for robust plasma operation at high humidity, J. Phys. D: Appl. Phys. 56 (34) (2023) 1–15, http://dx.doi.org/10.1088/1361-6463/acd2e4.

[47] A. Waskow, L. Ibba, M. Leftley, A. Howling, P.F. Ambrico, I. Furno, An in situ FTIR study of DBD plasma parameters for accelerated germination of *Arabidopsis thaliana seeds*, Int. J. Mol. Sci. 22 (21) (2021) 11540, http://dx.doi.org/10.3390/ijms222111540.

[48] L. Ibba, R. Agus, F. Avino, I. Furno, P. Ambrico, *In-situ* FTIR and laser induced fluorescence RONS characterization of atmospheric pressure nanosecond-pulsed surface DBD plasma for indirect treatments of *E.coli*, Plasma Chem. Plasma Process. (2024) 1–21., http://dx.doi.org/10.1007/s11090-023-10442-8.

[49] Bruker, Bruker VERTEX 80/80v FT-IR Spectrometers. URL https://www.bruker.com/en/products-and-solutions/infrared-and-raman/ft-ir-research-spectrometers/vertex-research-ft-ir-spectrometer/vertex-80-80v-ft-ir-spectrometer.html.

[50] E. Vervloessem, M. Gromov, N. De Geyter, A. Bogaerts, Y. Gorbanev, A. Nikiforov, NH_3 and HNOx formation and loss in nitrogen fixation from air with water vapor by nonequilibrium plasma, ACS Sustain. Chem. Eng. 11 (10) (2023) 4289–4298, http://dx.doi.org/10.1021/acssuschemeng.3c00208.

[51] HITRAN, HITRAN database, URL https://hitran.tsu.ru/.

[52] Y. Sakiyama, D.B. Graves, H.W. Chang, T. Shimizu, G.E. Morfill, Plasma chemistry model of surface microdischarge in humid air and dynamics of reactive neutral species, J. Phys. D: Appl. Phys. 45 (42) (2012) 425201, http://dx.doi.org/10.1088/0022-3727/45/42/425201.

[53] Metrohm, 914 pH/Conductometer, URL https://www.metrohm.com/de_ch/products/2/9140/29140020.html.

[54] Merckmillipore, Hydrogen Peroxide test 118789 product description, URL https://www.merckmillipore.com/CH/en/product/Hydrogen-Peroxide-Test,MDA_CHEM-118789.

[55] Merckmillipore, Nitrate Cell Test 114563 product description, URL https://www.merckmillipore.com/CH/en/product/Nitrate-Cell-Test,MDA_CHEM-114563#anchor_TI.

[56] Merckmillipore, Nitrite Cell Test 100609 product description, URL https://www.merckmillipore.com/CH/en/product/Nitrite-Cell-Test,MDA_CHEM-100609#anchor_CERT.

[57] Merckmillipore, Ozone Test 100607 product description, URL https://www.merckmillipore.com/CH/en/product/Ozone-Test,MDA_CHEM-100607.

[58] Merck, website, URL https://www.sigmaaldrich.com/CH/en.

[59] G. Sezonov, D. Joseleau-Petit, R. D'Ari, *Escherichia coli* physiology in Luria-Bertani broth, J. Bacteriol. 189 (23) (2007) 8746–8749, http://dx.doi.org/10.1128/JB.01368-07.

[60] S.J. Hagen, Exponential growth of bacteria: Constant multiplication through division, Amer. J. Phys. 78 (12) (2010) 1290–1296, http://dx.doi.org/10.1119/1.3483278.

[61] A.R. Tuttle, N.D. Trahan, M.S. Son, Growth and maintenance of *Escherichia coli* laboratory strains, Curr. Prot. 1 (1) (2021) 1–13, http://dx.doi.org/10.1002/cpz1.20.

[62] T.A. Devries, M.A. Hamilton, Estimating the antimicrobial log reduction: Part 1. Quantitative assays, Quant. Microbiol. 1 (1999) 29–45, http://dx.doi.org/10.1023/A:1010072226737.

[63] T.F. Scientific, website, URL https://www.thermofisher.com/ch/en/home.html.

[64] H. Motulsky, Intuitive Biostatistics: A Nonmathematical Guide to Statistical Thinking, Oxford University Press, 2018, URL https://books.google.ch/books?id=zxi2swEACAAJ.

[65] F. Zhang, X. Tang, L. Li, Origins of baseline drift and distortion in Fourier transform spectra, Molecules 27 (13) (2022) 1–13, http://dx.doi.org/10.3390/molecules27134287.

[66] M.J. Pavlovich, H.W. Chang, Y. Sakiyama, D.S. Clark, D.B. Graves, Ozone correlates with antibacterial effects from indirect air dielectric barrier discharge treatment of water, J. Phys. D: Appl. Phys. 46 (14) (2013) 145202, http://dx.doi.org/10.1088/0022-3727/46/14/145202.

[67] K. Kučerová, Z. Machala, K. Hensel, Transient spark discharge generated in various N2/O2 gas mixtures: Reactive species in the gas and water and their antibacterial effects, Plasma Chem. Plasma Process. 40 (3) (2020) 749–773, http://dx.doi.org/10.1007/s11090-020-10082-2.

[68] L.O. Melnik, V.F. Vakulenko, M.M. Saprykina, A.M. Sova, Change of the oxidation-reduction potential of model and natural waters in the ozone disinfection process, J. Water Chem. Technol. 43 (1) (2021) 85–91, http://dx.doi.org/10.3103/s1063455x21010094.

[69] L.T. Fan, B.C. Shen, S.T. Chou, The surface-renewal theory of interphase transport: a stochastic treatment, Chem. Eng. Sci. 48 (23) (1993) 3971–3982, http://dx.doi.org/10.1016/0009-2509(93)80376-2.

[70] B.I. Morsi, O.M. Basha, Mass transfer in multiphase systems, in: M. Solecki (Ed.), Mass Transfer, IntechOpen, Rijeka, 2015, http://dx.doi.org/10.5772/60516, Ch. 9.

[71] B. Tarabová, P. Lukeš, M. Janda, K. Hensel, L. Šikurová, Z. Machala, Specificity of detection methods of nitrites and ozone in aqueous solutions activated by air plasma, Plasma Process. Polym. 15 (6) (2018) e1800030, http://dx.doi.org/10.1002/ppap.201800030.

[72] C. von Sonntag, U. von Gunten, Chemistry of Ozone in Water and Wastewater Treatment: From Basic Principles to Applications, 2015, pp. 14–17, http://dx.doi.org/10.2166/9781780400839.

[73] E. Feizollahi, U. Basu, R. Fredua-Agyeman, B. Jeganathan, L. Tonoyan, S.E. Strelkov, T. Vasanthan, A.G. Siraki, M.S. Roopesh, Effect of plasma-activated water bubbles on *Fusarium graminearum*, deoxynivalenol, and germination of naturally infected barley during steeping, Toxins 15 (2) (2023) 124, http://dx.doi.org/10.3390/toxins15020124.

[74] J. Julák, V. Scholtz, S. Kotúčová, O. Janoušková, The persistent microbicidal effect in water exposed to the corona discharge, Phys. Med. 28 (3) (2012) 230–239, http://dx.doi.org/10.1016/j.ejmp.2011.08.001.

[75] B. Choudhury, S. Portugal, N. Mastanaiah, J.A. Johnson, S. Roy, Inactivation of *Pseudomonas aeruginosa* and methicillin-resistant *Staphylococcus aureus* in an open water system with ozone generated by a compact, atmospheric DBD plasma reactor, Sci. Rep. 8 (1) (2018) 1–11, http://dx.doi.org/10.1038/s41598-018-36003-0.

[76] R. Sander, Compilation of Henry's law constants (version 4.0) for water as solvent, Atmos. Chem. Phys. 15 (8) (2015) 4399–4981, http://dx.doi.org/10.5194/acp-15-4399-2015.

[77] J. Hoigné, H. Bader, W.R. Haag, J. Staehelin, Rate constants of reactions of ozone with organic and inorganic compounds in water-III. Inorganic compounds and radicals, Water Res. 19 (8) (1985) 993–1004, http://dx.doi.org/10.1016/0043-1354(85)90368-9.

[78] K.N. Jordan, L. Oxford, C.P. O'Byrne, Survival of low-pH stress by *Escherichia coli* O157:H7: Correlation between alterations in the cell envelope and increased acid tolerance, Appl. Environ. Microbiol. 65 (7) (1999) 3048–3055, http://dx.doi.org/10.1128/aem.65.7.3048-3055.1999.

[79] P. Small, D. Blankenhorn, D. Welty, E. Zinser, J.L. Slonczewski, Acid and base resistance in *Escherichia coli* and *Shigella flexneri*: Role of rpoS and growth pH, J. Bacteriol. 176 (6) (1994) 1729–1737, http://dx.doi.org/10.1128/jb.176.6.1729-1737.1994.

[80] E. Riordan, N. Minogue, D. Healy, P. O'Driscoll, J.R. Sodeau, Spectroscopic and optimization modeling study of nitrous acid in aqueous solution, J. Phys. Chem. A 109 (5) (2005) 779–786, http://dx.doi.org/10.1021/jp040269v.

[81] B. He, Y. Ma, X. Gong, Z. Long, J. Li, Q. Xiong, H. Liu, Q. Chen, X. Zhang, S. Yang, Q.H. Liu, Simultaneous quantification of aqueous peroxide, nitrate, and nitrite during the plasma-liquid interactions by derivative absorption spectrophotometry, J. Phys. D: Appl. Phys. 50 (44) (2017) 445207, http://dx.doi.org/10.1088/1361-6463/aa8819.

[82] Z. Machala, B. Tarabova, K. Hensel, E. Spetlikova, L. Sikurova, P. Lukes, Formation of ROS and RNS in water electro-sprayed through transient spark discharge in air and their bactericidal effects, Plasma Process. Polym. 10 (7) (2013) 649–659, http://dx.doi.org/10.1002/ppap.201200113.

[83] Y. Zhou, A. Oehmen, M. Lim, V. Vadivelu, W.J. Ng, The role of nitrite and free nitrous acid (FNA) in wastewater treatment plants, Water Res. 45 (15) (2011) 4672–4682, http://dx.doi.org/10.1016/j.watres.2011.06.025.

[84] M. Chislett, J. Guo, P.L. Bond, Y. Wang, B.C. Donose, Z. Yuan, Reactive nitrogen species from free nitrous acid (FNA) cause cell lysis, Water Res. 217 (2022) 118401, http://dx.doi.org/10.1016/j.watres.2022.118401.

[85] M. Chislett, Z. Yu, B.C. Donose, J. Guo, Z. Yuan, Understanding the effect of free nitrous acid on biofilms, Environ. Sci. Technol. 56 (16) (2022) 11625–11634, http://dx.doi.org/10.1021/acs.est.2c01156.

[86] Y. Li, J. Pan, G. Ye, Q. Zhang, J. Wang, J. Zhang, J. Fang, In vitro studies of the antimicrobial effect of non-thermal plasma-activated water as a novel mouthwash, European Journal of Oral Sciences 125 (6) (2017) 463–470, http://dx.doi.org/10.1111/eos.12374.

[87] A. Lavrikova, N.C.T. Dadi, H. Bujdáková, K. Hensel, Inactivation pathways of *Escherichia coli* and *Staphylococcus aureus* induced by transient spark discharge in liquids, Plasma Process. Polym. (2024) http://dx.doi.org/10.1002/ppap.202300147.

[88] Y. Bai, A. Idris Muhammad, Y. Hu, S. Koseki, X. Liao, S. Chen, X. Ye, D. Liu, T. Ding, Inactivation kinetics of *Bacillus cereus* spores by plasma activated water (PAW), Food Res. Int. 131 (2020) 109041, http://dx.doi.org/10.1016/j.foodres.2020.109041.

[89] M. Kostakioti, M. Hadjifrangiskou, S.J. Hultgren, Bacterial biofilms: Development, dispersal, and therapeutic strategies in the dawn of the postantibiotic era, Cold Spring Harb. Perspect. Med. 3 (4) (2013) 1–23, http://dx.doi.org/10.1101/cshperspect.a010306.

[90] R. Zhou, R. Zhou, P. Wang, B. Luan, X. Zhang, Z. Fang, Y. Xian, X. Lu, K.K. Ostrikov, K. Bazaka, Microplasma bubbles: Reactive vehicles for biofilm dispersal, ACS Appl. Mater. Interfaces 11 (23) (2019) 20660–20669, http://dx.doi.org/10.1021/acsami.9b03961.

[91] R. Kastl, website, URL https://www.souffleurdeverre.ch/.